Bulletin of the Seismological Society of America, Vol. 93, No. 6, pp. 2649–2663, December 2003

Estimating Slab Earthquake Response Spectra from a 3D *Q* Model

by Donna Eberhart-Phillips and Graeme McVerry

Abstract The problem of estimating response spectra for a heterogeneous lithosphere can be addressed by directly computing attenuation from physical models. In a subduction zone, slab earthquakes will have different attenuation through the mantle wedge than the slab. This article is primarily concerned with very high loss paths through the attenuating mantle underlying the volcanic zone of the North Island, New Zealand, where low *Q* requires modification of the "standard" New Zealand engineering response spectrum model.

A lack of strong-motion data prevents a standard regression analysis for paths from deep slab earthquakes through the highly attenuating mantle zone. Instead, modifications have been derived using a 3D frequency-independent *Q* model that has been developed for the North Island subduction zone from 2–20 Hz local earthquake t^* data. By calibrating the t^* crustal results to the standard New Zealand model, amplitudes can be compared between the standard model and the 3D *Q* model. Additional path-averaged attenuation rate coefficients, *CQ*, for each source and station pair are determined. This results in simple expressions for *CQ* as a function of centroid depth, for modifying the standard model.

This modification reduces the model spectra by a factor of approximately 2–4 for mantle wedge paths below the volcanic region. This reduction is similar to the observed variation in response spectra, at periods below 0.4 sec, for a 160-km-deep M_w 6.0 earthquake. For shallow earthquakes propagating through the shallow volcanic region, the new model gives results that are similar to a volcanic-path attenuation term derived by regression analysis.

Introduction

It is important for engineering prediction of earthquake ground motion to model the heterogeneous transmission of shaking from deep slab earthquakes in New Zealand. The North Island lies above the Hikurangi subduction zone (Fig. 1), which has resulted in volcanism and extension in the Taupo volcanic zone (TVZ). Because of along-strike variation in plate motion and plate-interface properties, the TVZ is limited to the central and northern portions of the North Island, although the subducted slab continues to the northern South Island (Reyners, 1998; Eberhart-Phillips *et al.*, 2002; Upton *et al.*, 2002). Seismograms from mantle paths indicate high attenuation compared to slab paths, yet there are not enough strong-motion data to use a standard regression approach to model the attenuation in the mantle.

The geometry for deep earthquakes is illustrated schematically in Figure 2a. Below 40-km depth, earthquakes tend to occur only in the subducting slab and hence are located directly below the TVZ. The subducting Pacific plate slab has very low attenuation, the crust of the Australian plate has moderate attenuation, and the mantle wedge between the slab and the overlying crust has very high attenuation. Additionally the crust in the TVZ has very high attenuation. Thus deep earthquakes will be more strongly felt at more distant eastern sites with low-loss slab paths, such as Napier, than at closer sites with paths through the mantle wedge. Deep earthquakes have produced triggered strong-motion records at eastern sites, but for engineering applications the response for deep earthquakes at sites including high-loss paths, such as Taupo and Rotorua in the TVZ and other locations to the northwest, must also be estimated.

The effect of high attenuation in the mantle and TVZ can be clearly seen in both felt and instrumental data. An atlas of isoseismal maps for New Zealand (Downes, 1995) contains several deep-earthquake maps for which the major axis of the ellipse that fits the isoseismal pattern is displaced well to the east of the epicenter (Fig. 2b). These maps of felt effects provide insight for earthquakes that lack strong-motion records. Although not formally mapped, the same effect can be seen in records from strong-motion accelerographs. For several deep earthquakes in the general vicinity of the TVZ, the strongest accelerations have been recorded in the vicinity of Napier and Gisborne, whereas instruments at sites above or west of the epicenter have either not been triggered or have returned weaker motions.

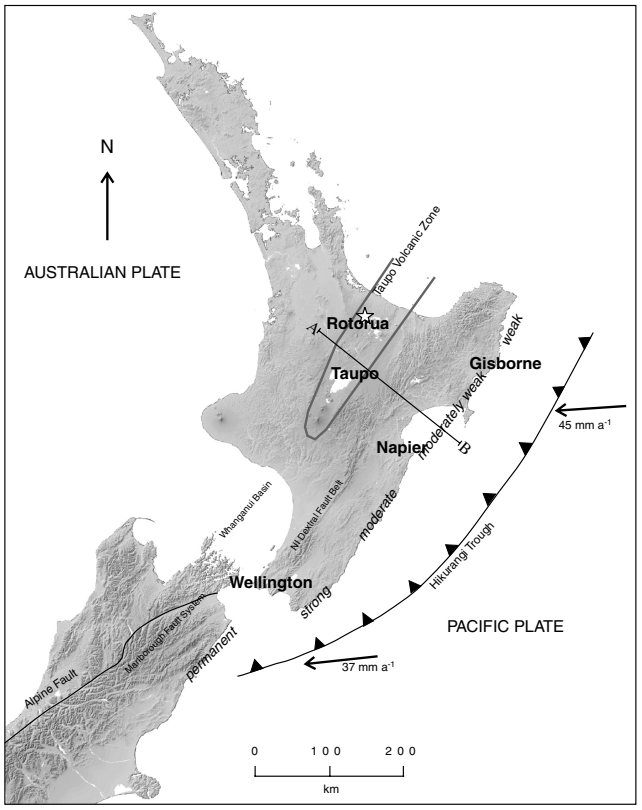

Figure 1. Generalized tectonics of the North Island of New Zealand. The region is dominated by oblique subduction of the Pacific plate along the Hikurangi Trough, with plate velocity indicated by arrows. The outlined Taupo volcanic zone (TVZ) exhibits active volcanism and rifting. The transcurrent plate motion is expressed in upper plate fault zones such as the North Island dextral fault belt. The coupling along the plate interface has been shown by Reyners (1998) to vary from weak to strong as labeled, becoming permanent in the South Island as the tectonic style switches to oblique continental collision. The star indicates the epicenter of the earthquake displayed in Figure 4. Line AB shows the cross section for attenuation (Fig. 7).

Dowrick and Rhoades (1999) have developed attenuation models for modified Mercalli intensity isoseismals for New Zealand earthquakes, including a model for earthquakes more than 70 km deep. Regardless of the actual location of the deep event, they find that the isoseismals are systematically shifted to the east (shown by the AA line in Figure 2a) rather than being centered around the epicenter as might be expected without lateral heterogeneity in the crust and upper mantle. The offset at the center of the isoseismal pattern from the epicenter is demonstrated by the 173-km-deep earthquake shown in Figure 2. The AA line corresponds to the 35-km depth contour on the top of the dipping slab and thus means that the isoseismals for all deep earthquakes are centered east of the mantle wedge. The shape of the isoseismals is modeled as an asymmetric ellipse compressed on the western side near the TVZ. The exact shape varies with the magnitude and depth.

The standard New Zealand subduction zone response spectrum attenuation model (McVerry *et al.*, 2000) is derived from data exhibiting the behavior shown in Figure 2. There are not enough strong-motion data to use a standard regression approach to model the attenuation for paths through the mantle. The film-recording accelerographs that made up the New Zealand strong-motion network until the recent introduction of digital accelerographs and digital seismographs were too insensitive to yield more than a few useful records of motions from paths through the attenuating mantle. In fact, these few records were excluded from the regression analysis so as not to corrupt the models for the much more commonly recorded paths up the slab. The practical problem for hazard analysis is that it is nonconservative to simply ignore contributions from deep slab earthquakes at sites involving mantle paths. However, using the standard model, which is appropriate for paths up the slab to sites in the eastern or southern North Island, for sites above the source zone of deep slab earthquakes involving mantle paths, produces overly high estimated motions that incorrectly dominate the hazard estimates.

In the Hokkaido region of Japan, there is similarly a problem of varied intensity for deep earthquakes depending on the path through the low-Q mantle wedge. Takai *et al.* (2000) developed a method to predict intensity based on path length through the mantle wedge. They used a simple two-element Earth model with slab and wedge. Then they undertook a regression using path length in each layer, without solving for Q.

We aim to go a step further with a physical modeling approach, taking a 3D Earth model and using it to develop a modified response spectral model that accounts for heterogeneous structure. The spectral attenuation of small earthquakes (magnitude ≥ 2.5), which are routinely recorded by the seismograph network, can be parameterized by t^*, as described later. The t^* data are inverted for a 3D Q model. Using the Q model, attenuation is calculated along various 3D ray paths. Finally attenuation rate terms are determined that fit into the response spectral model, with the other terms in the model being held constant.

We make the assumption that Q measured for small earthquakes will be applicable to large earthquakes. While the amplification of ground motion in soft soil is known to be nonlinear with magnitude (Beresnev and Wen, 1996), there is little reason to expect Q would vary with magnitude. For fluid-saturated porous media with low effective stress, where attenuation results from localized fluid flow and grain-contact effects, some studies indicate that Q decreases for large strain amplitudes ($>10^{-6}$) that disturb the grain contacts (Sharma and Tutuncu, 1994; Winkler and Murphy, 1995). The strain amplitude for a magnitude >7.0 earthquake at 100-km distance could reach 10^{-6} (Gomberg, 1996), and thus there is some possibility of strain-related Q decrease. It is less clear how the attenuation mechanisms

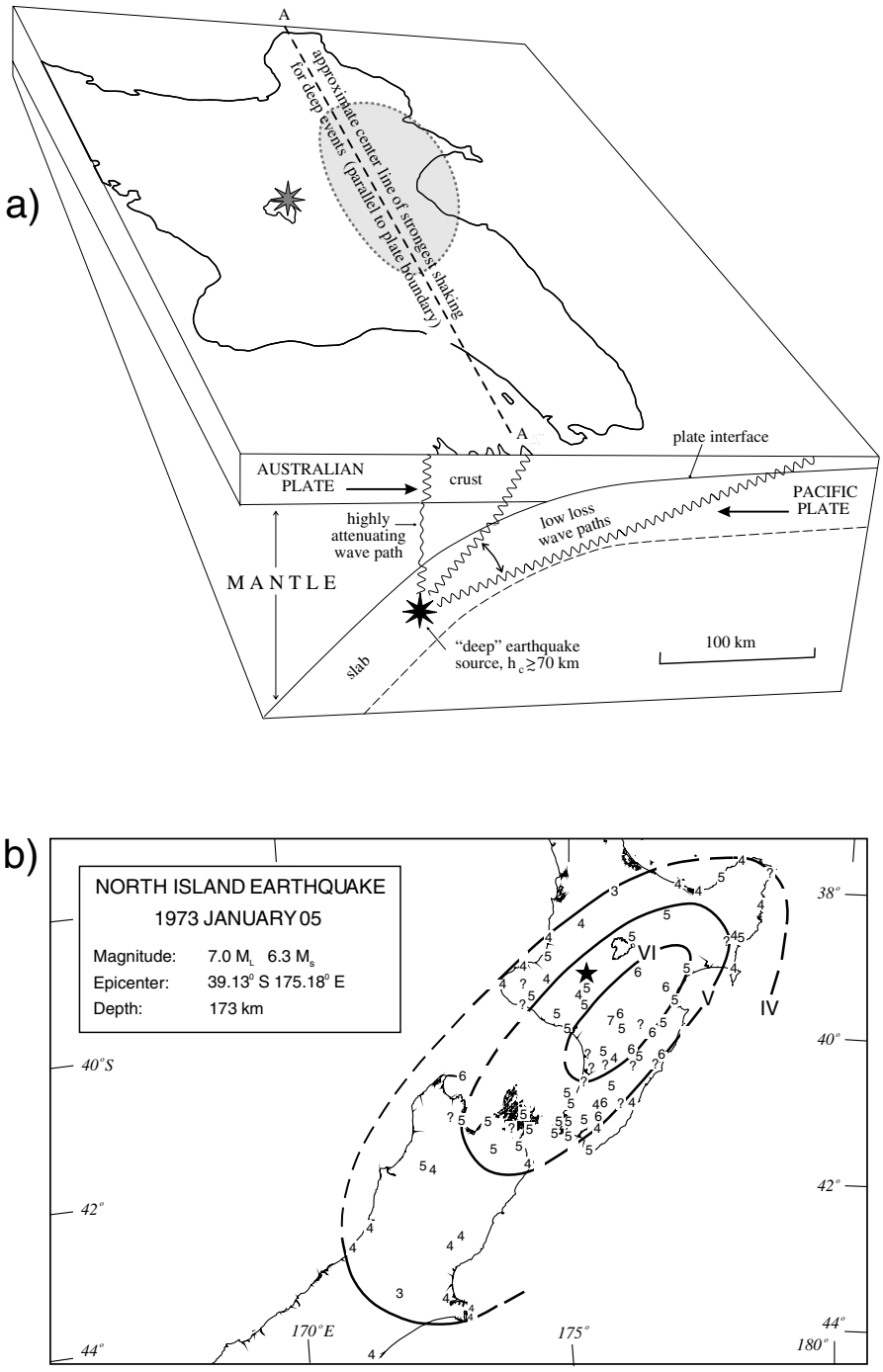

Figure 2. (a) Schematic view comparing highly attenuating mantle paths to sites above the focus of a deep earthquake, with low-loss paths up the subducting slab and through the crust to sites east of the epicenter (after Dowrick and Rhoades, 1999). The markedly higher attenuation rate for mantle paths causes isoseismal patterns to be asymmetric and offset to the east of the epicenter, as illustrated by the shaded ellipse. Black star, hypocenter; gray star, epicenter. (b) An example of an isoseismal pattern from a deep earthquake offset to the east of its epicenter, marked by a star (Downes, 1995).

work in the more viscous mantle wedge, but they are likely to be less influenced by strain amplitude.

New Zealand Standard Response Spectral Model

The standard New Zealand response spectral acceleration model (McVerry *et al.*, 2000) was obtained by an empirical fit to observed spectra using standard regression models. The model took account of different tectonic types of earthquakes and their depths and mechanisms. The base data consisted of 5% damped horizontal acceleration response spectra SA(T) from a data set of New Zealand earthquake records, supplemented by peak ground acceleration (PGA) values from overseas records in the near-source range. Limited ranges of magnitude and distance and insufficient records in the response spectrum data set prevented the development of a purely New Zealand model. Instead, international models were adjusted to better fit the New Zealand data. Abrahamson and Silva (1997) was selected as a suitable base model for crustal earthquakes and Youngs *et al.* (1997) for subduction-zone earthquakes.

The form of the McVerry *et al.* (2000) model for crustal earthquakes at weak rock sites is

$$\begin{aligned}\ln \mathrm{SA}(T)_{\text{standard NZ crustal}} = \\ & C_1(T) + C_{4\mathrm{AS}}(M - 6) \\ & + C_{3\mathrm{AS}}(T)\,(8.5 - M)^2 + C_5(T)\,r \\ & + (C_8(T) + C_{6\mathrm{AS}}(M - 6)) \\ & \ln(r^2 + C_{10\mathrm{AS}}{}^2(T))^{1/2} + C_{46}(T)\,r_{\mathrm{VOL}},\end{aligned} \tag{1}$$

where T is period, M is moment magnitude, r is the slant distance (straight-line path) from the site to the fault, and r_{VOL} is the length of the part of the source-to-site path that lies in the volcanic zone. Other terms for mechanism and site classification may be included. Coefficients subscripted "AS" were constrained to the base model (Abrahamson and Silva, 1997) values.

The model contains two anelastic attenuation coefficients, C_5 and C_{46}, which vary with period. The average crustal attenuation rate is modeled by C_5. However this does not account for the recognized high attenuation in the volcanic region of the North Island (Haines, 1981; Cousins *et al.*, 1999). For shallow earthquakes with paths through the high-attenuation-rate crustal volcanic region, there are sufficient data to derive volcanic-path anelastic attenuation terms for the standard model using regression analyses. The different volcanic crustal attenuation rate is modeled by C_{46}. For PGA, $C_5 = -0.00967$ km^{-1}, while $C_{46} = -0.03279$ km^{-1}, that is, a total rate of -0.04246 km^{-1}, over 4 times the standard crustal rate.

The form of the McVerry *et al.* (2000) model for subduction-zone earthquakes for weak rock sites is

$$\begin{aligned}\ln \mathrm{SA}(T)_{\text{standard NZ subduction zone}} = \\ & C_{11}(T) + C_{12}(T)\,(\mathrm{M} - 6) + C_{13\mathrm{Y}}(T)\,(10 - \mathrm{M})^3 \\ & + C_{17}(T)\ln(r + C_{18\mathrm{Y}}\exp(C_{19\mathrm{Y}}\,M)) \\ & + C_{20}(T)\,H_{\mathrm{C20}} + C_{24}(T)\,\mathrm{SI} + C_{46}(T)\,\mathrm{r_{VOL}}\,(1 - \mathrm{DS})\end{aligned} \tag{2}$$

where SI = 1 for subduction interface earthquakes or zero otherwise, H_{C20} is the lesser of the centroid depth or 150 km, and DS is 1 for deep slab earthquakes (centroid depths greater than 50 km) or zero otherwise. The coefficients subscripted "Y" were constrained to their values in the Youngs *et al.* (1997) model. There was also a near-source constraint that the magnitude dependence at zero distance is the same as for the Youngs *et al.* model, requiring

$$C_{12}(T) + C_{17}(T)\,C_{19\mathrm{Y}} = C_{12\mathrm{Y}} + C_{17\mathrm{Y}}(T)\,C_{19\mathrm{Y}}\,. \tag{3}$$

This model is similar to the Youngs *et al.* model, but allows the coefficients of the magnitude, centroid depth, and subduction interface terms to be functions of period, as well as adding the volcanic path anelastic attenuation term $C_{46}(T)$ r_{VOL} for interface and shallow slab earthquakes with crustal volcanic-zone paths.

The resulting PGA attenuation curves for shallow subduction-zone earthquakes for shallow soil sites are very similar to the Youngs *et al.* (1997) rock curves (Fig. 3), for both earthquakes at the subduction interface and in the shallow slab (i.e., at centroid depths around 20 km). For deeper slab earthquakes, the New Zealand model predicts greater shallow soil PGAs than the Youngs *et al.* (1997) rock model.

The similarity between the Youngs *et al.* (1997) rock curves and the New Zealand shallow soil curves can be explained in terms of the site classification used in the two models. The New Zealand site classifications vary from those used in the Abrahamson and Silva (1997) and Youngs *et al.* (1997) attenuation models, especially for the rock classes. The Abrahamson and Silva (1997, p. 95) "rock" class includes both "rock ($V_s > 600$ m/s) or very thin soil (<5m) over rock" and "shallow soil; soils 5–20 m thick over rock." In describing their rock class, Youngs *et al.* (1997, p. 59) stated that "rock site conditions are expected to be similar to typical rock conditions in the California strong motion database, consisting of at most a few feet of soil over weathered rock." N. A. Abrahamson (personal comm., 2003) stated that the rock classes in both the Abrahamson and Silva (1997) and Youngs *et al.* (1997) models are in fact similar, representing both rock and shallow soil sites. The New Zealand rock class requires material with a compressive strength exceeding 1 MPa, although allowing a surface layer of no more than 3 m depth of highly weathered or completely weathered rock or soil. Although the classification can be made from geological descriptions rather than requiring measurement of the strength, and in practice is assigned this way, the minimum strength of 1 MPa corresponds to the boundary between rock and soil defined by the New Zealand

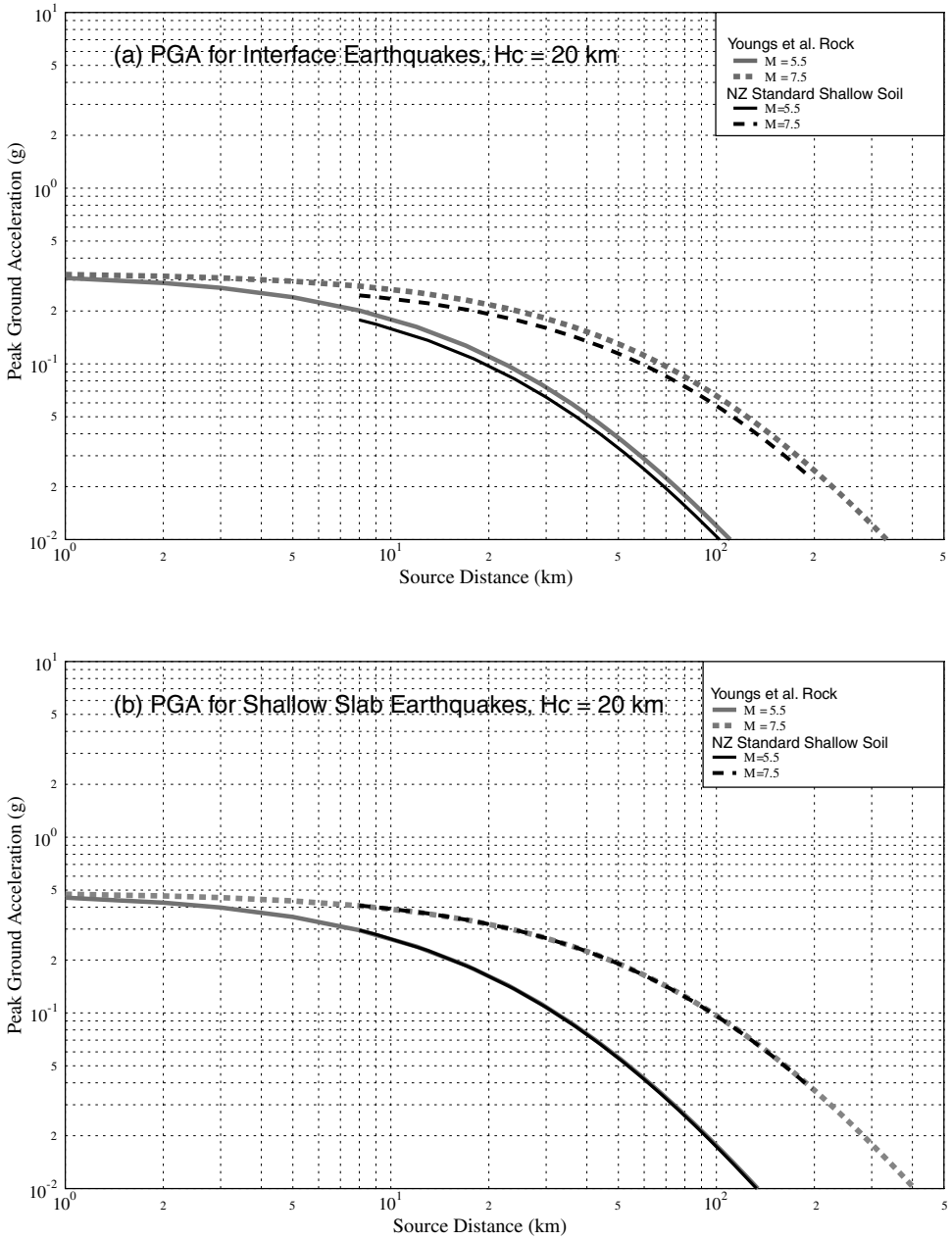

Figure 3. Comparison, for shallow subduction earthquakes, of the New Zealand standard shallow soil model (black lines, McVerry *et al.,* 2000) to the worldwide model (gray lines, Youngs *et al.,* 1997), which was derived from both rock and shallow soil sites. Peak ground acceleration is for *M* 5.5 (solid lines) and *M* 7.5 (dashed lines) earthquakes with centroid depth of 20 km. (a) Plate interface earthquakes; (b) shallow slab earthquakes.

Geomechanics Society (1988), and materials assigned to this class are clearly rock rather than soil. The separation of rock sites from shallow soil sites was found to be statistically justified in the development of the New Zealand response spectrum attenuation relations, with shallow soil sites typically having stronger spectra than the rock sites that are lumped with them in the Abrahamson and Silva (1997) model and reportly in the Youngs *et al.* (1997) model also. Rodriguez-Marek *et al.* (2001) have pointed out that the Abrahamson and Silva (1997) rock (and shallow soil) class is in fact dominated by records from shallow soil sites, and their spectra reflect this, representing those for shallow soil sites rather than the considerably reduced spectra from rock sites, similar to the comparisons between rock spectra and shallow soil site spectra in New Zealand. It is therefore not surprising that the Youngs *et al.* (1997) rock PGA attenuation

curves are similar to the shallow soil rather than rock curves from the New Zealand model.

The McVerry *et al.* (2000) model for subduction-zone earthquakes includes a term for hypocentral depth, $C_{20}\,H_C$. This coefficient is positive (e.g., 0.013 for 2 Hz) and thus serves to increase the anticipated acceleration for deep earthquakes relative to shallower earthquakes that have the same distance. However this is a biased result, because available strong-motion records involved low-loss paths within the subducted slab. With such limited data, empirical regression methods will predict high accelerations for all deep earthquakes and thus will overestimate nonslab paths. The high attenuation for deep slab earthquakes for propagation paths through the mantle wedge has been recognized for many years (e.g., Mooney, 1970), but scarcity of strong-motion data for the effected paths prevented its modeling in the McVerry *et al.* (2000) regression-based attenuation expression.

Heterogeneous Q Model

The New Zealand National Seismograph Network records earthquakes of magnitude 3.5 and greater. These data are available for numerous earthquakes that were too small to trigger strong-motion recorders. Deep earthquake recordings show large differences between eastern stations with slab paths and other stations with paths through the mantle wedge and volcanic zone.

Records for a 180-km-deep M 4.7 earthquake under Rotorua (star in Fig. 1) are shown in Figure 4, with a vertical-component velocity seismogram and observed and modeled amplitude spectra for each station. TVZ stations are compared to eastern stations, illustrating that the dropoff in amplitude with frequency is much more pronounced for the TVZ stations. We fit each velocity amplitude spectra (equation 4) with three parameters: the spectral level, Ω_0, corner frequency, f_c, and t^*, a parameter that represents the whole-path attenuation (Scherbaum, 1990; Rietbrock, 2001; Eberhart-Phillips and Chadwick, 2002).

$$A(f) = 2\pi f\Omega_0 * \frac{f_c^2}{(f_c^2 + f^2)} * \exp[-\pi f t^*] \qquad (4)$$

Amplitude spectra for a window (2.56 sec) around the P arrival are used, including only data with significant a signal-to-noise ratio (>2) over the frequency band 1–20 Hz. In the 3D Q_P inversion, the 3D V_p model is used in determining ray paths and in computing Q_P perturbations. The corner frequency, f_c, of the event is estimated by a grid search using all the recordings for each event. Then an iterative procedure is used to fit the spectral level, Ω_0, and t^*. In order to weight each t^* residual in the Q_P inversion, we estimate a quality for the t^* observation based on how well the spectra is modeled and the range of frequency that is modeled. Thus Figure 4 shows the t^* values that describe the varied frequency decay, with t^* being roughly 3 times greater for the TVZ stations than for the eastern stations.

Given t^* for a set of earthquakes and stations and a 3D velocity structure, t^* can be inverted for Q structure by relating t^* to Q along the ray paths (s).

$$t^* = \int_{\text{raypath}} 1/(Q(s) * V(s))ds \qquad (5)$$

This method has been used to obtain detailed 3D Q_P models for regions with dense temporary seismograph deployments (Rietbrock, 2001; Eberhart-Phillips and Chadwick, 2002). A t^* station term can optionally be included in equation 5, but since the application in this study is for predicting the attenuation rate, we choose to push near-surface attenuation effects into the 3D model.

For estimating the heterogeneous attenuation of deep earthquakes under the North Island, we compute a larger scale 3D Q_P model using primarily the sparse permanent network. For the period 1990–2000, we selected 450 earthquakes, magnitude 4–6, near-surface to 400-km depth, that were spatially well distributed and recorded on at least 12 stations. Seismograms from all 146 available stations were used, but most of those stations were temporary and only 27 stations had 50 or more observations. The data comprised 10,475 P arrivals and 4473 t^* values. As t^* can only be estimated when the noise is low over the desired frequency range (Fig. 4), there are fewer t^* than P-arrival data. Since our goal was to image the mantle wedge, we did not include sources from the eastern North Island where the subducted slab is shallower than 50 km. The initial model was extrapolated from 3D studies of the eastern North Island (Eberhart-Phillips and Chadwick, 2002; Eberhart-Phillips *et al.*, 2002).

The inversion model is coarse 3D in the crust to 35-km depth with 11–75 km grid spacing, and 2D for 35- to 400-km depth through linking of along-strike nodes. Velocity and Q_P are linearly interpolated between nodes. The method assumes frequency-independent Q_P. Other linking of adjacent nodes was done within the mantle wedge to make its properties relatively uniform even on the less-resolved peripheral nodes. This is important for creating a model that is useful for attenuation applications while still making sure the model fits the data.

The results are shown in Figure 5 for a cross section from the east coast across the volcanic zone. The inversion hypocenters are also shown. The V_p model shows high velocity for the slab relative to the mantle wedge and reduced velocity for the mantle below the TVZ. The Q_P model shows high Q_P (500–900) for the subducted slab and low Q_P (100–200) for the mantle wedge. Low Q_P is also shown for the TVZ and the eastern accretionary sediments. Note that the low crustal Q_P on the west could be due to smearing along ray paths that primarily sample the mantle wedge since there are few crisscrossing peripheral crustal ray paths to independently resolve crustal velocity.

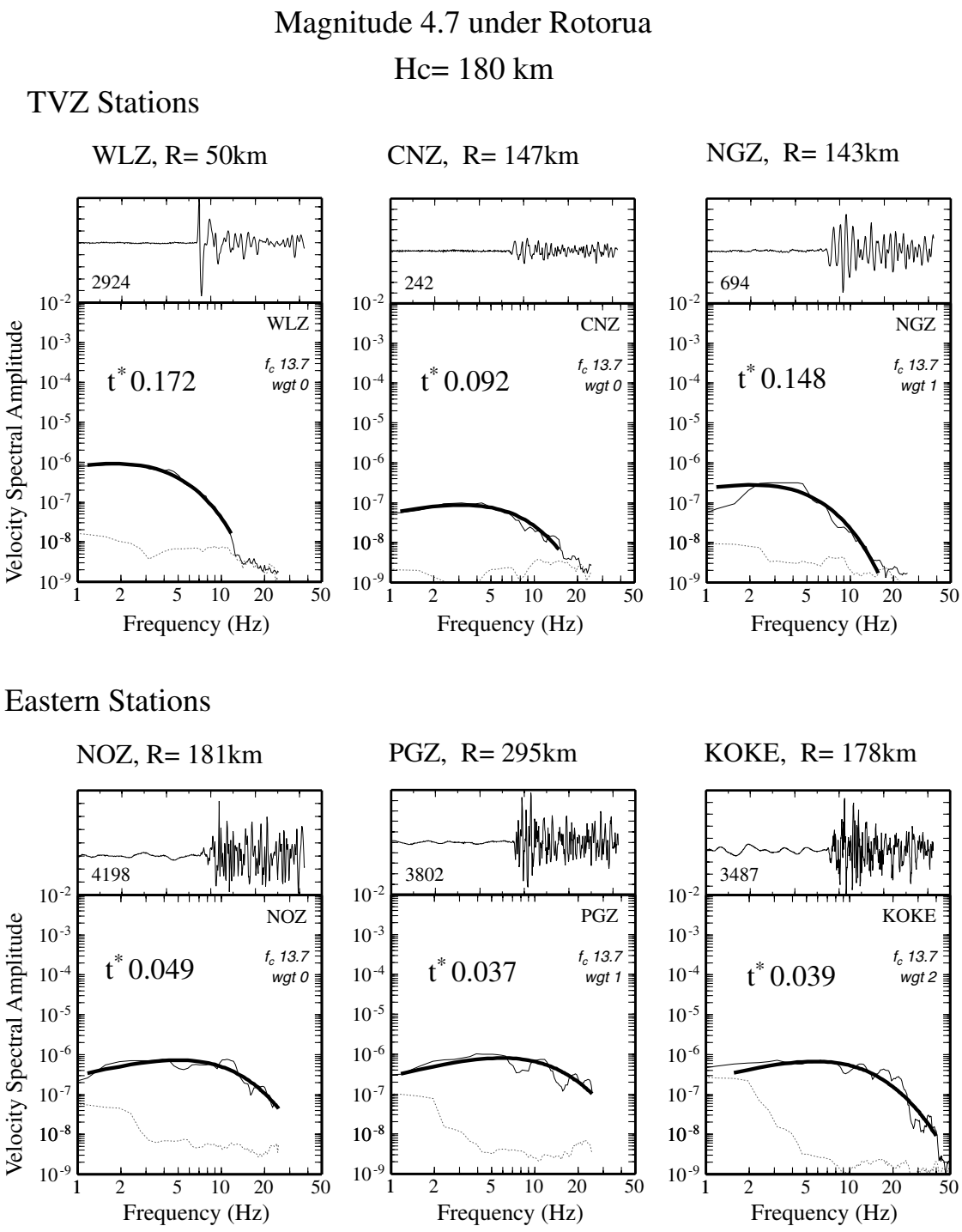

Figure 4. Example of fitting t^* for a 180-km-deep earthquake. TVZ stations, display more attenuated waveforms than eastern stations, which corresponds to much higher t^* values. For each station, the waveform is shown with the velocity spectra underneath. A common f_c is found for the event, and then the spectral level and t^* are estimated. Dotted lines show the noise spectra and heavy lines show the fit to the data over the range with adequate signal-to-noise ratio, and *wgt* indicates fit quality with best fit = 0.

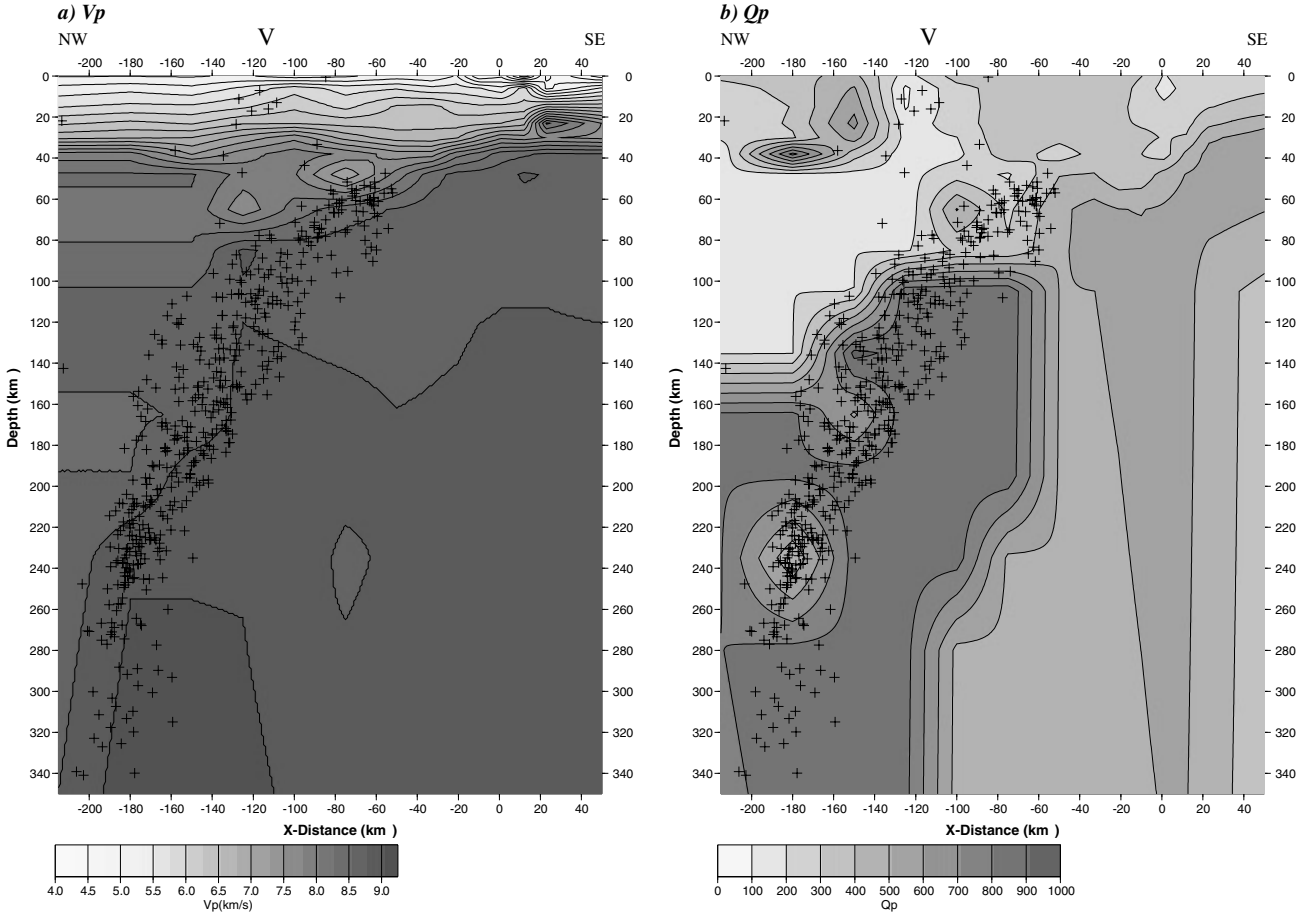

Figure 5. (a) V_p and (b) Q_p models along a cross section to 350-km depth through the volcanic zone, labeled "V". Hypocenters are shown by plus signs, all inversion earthquakes below 35 km where model is 2D, and hypocenters near this cross section above 35 km where model is coarse 3D.

The resolution pattern is shown by the computed diagonal resolution elements (Fig. 6). Since each set of linked nodes is treated as a single parameter in the inversion, all nodes in each set are shown with the resolution of that parameter. The resolution is good below 35-km depth and is low in the northwestern crust. The high-Q_p region at the base of the crust (40-km depth) in the northwestern region at $x = -180$ is realistic, although given the overlying low resolution, it is difficult to gauge its spatial extent.

The variability in slab Q_P may in part be due to 3D variability in slab shape and properties that are not well characterized by our sparse data and 2D slab model. In the future, data from additional temporary seismograph networks across the central North Island will make it possible to obtain a more detailed 3D Q_P model that will be more appropriate for structural interpretation. However, the small-scale slab Q_P variations do not have a large effect on attenuation rate. The coarse model presented here is adequate for application to estimating attenuation effects and determining whether it is feasible to modify response spectral relations using physical models.

Attenuation Rate Terms from 3D Q

Using the 3D Q_P model, anelastic attenuation rate terms need to be obtained that are functions of period and hypocentral depth in order to modify the standard response spectral attenuation model (i.e., the McVerry *et al.* [2000] model determined from regression analysis of strong-motion data, excluding data from paths through the highly attenuating zone of the mantle wedge).

$$\ln \mathrm{SA}(T) = \{\text{standard model}\} - CQ(T,H_c)\, r \quad (6)$$

We assume the *P*-wave Q_p is equivalent to the *S*-wave Q_s, as a wide range of Q_p/Q_s values are observed throughout the world from roughly 0.6 to 1.5 (Yoshimoto *et al.*, 1993), and using a different Q_p/Q_s value would not alter our final results. Thus in the following text "Q" $= Q_p = Q_s$ and "Q_1" is Q at 1 Hz. The local attenuation rate at 1 Hz is $\pi/(Q_1{*}V_s)$, plotted in Figure 7. This emphasises the effect of the volcanic zone, which has low Q and lower velocity than the mantle wedge. Synthetic t^* data are computed for a range

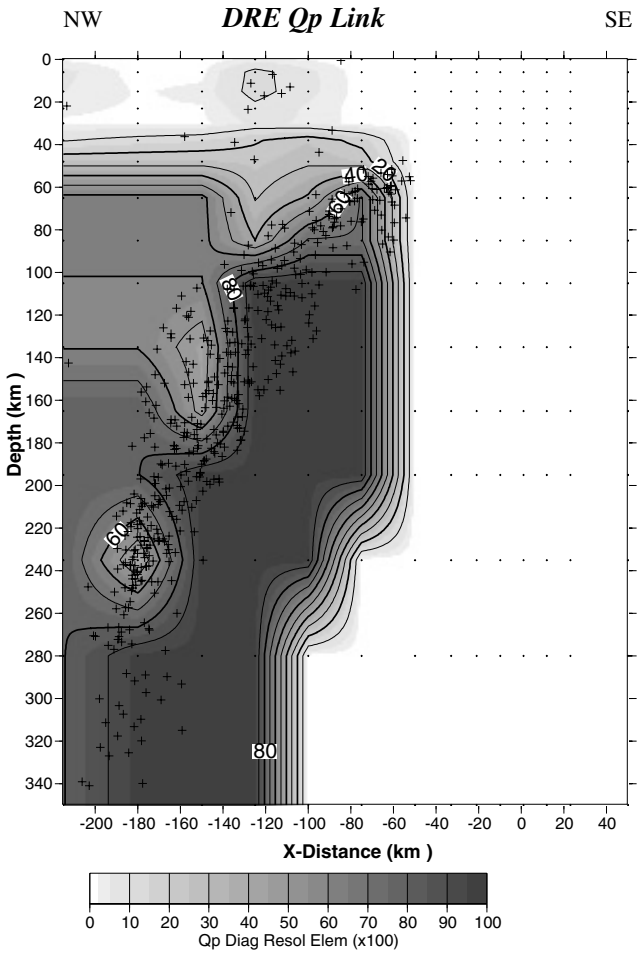

Figure 6. Plot of diagonal resolution elements for Q_p inversion (Fig. 5b). Note that the southeastern Q_p was fixed to previous models, the model is 2D below 35-km depth, and linking combines weakly sampled nodes in the inversion.

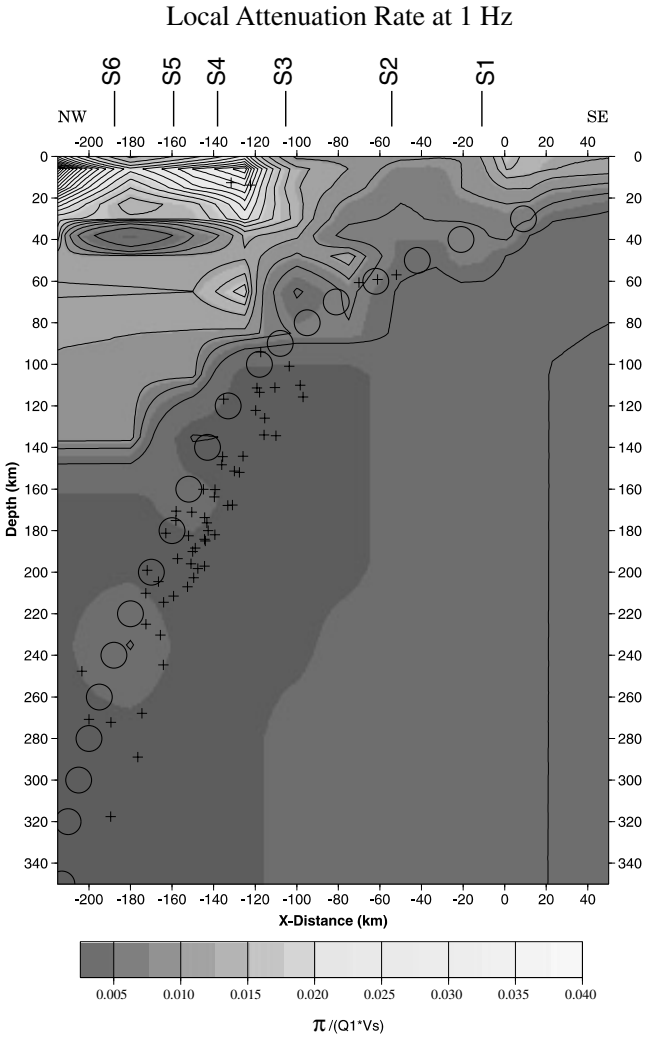

Figure 7. Cross section, along line AB in Figure 1, showing attenuation rate $[\pi/(Q_1{*}V_s)]$ at 1 Hz, and synthetic sources and sites used for computing attenuation terms $CQ(H_C)$. Sites are labeled S1–S6, circles are synthetic sources, and plus signs are inversion hypocenters. Note local attenuation rates of 0.002 in the deep slab, 0.007 in the standard crust (between S1 and S2), and 0.030 in the volcanic zone (below S4).

of sources and sites in order to estimate CQ. Sources are distributed from 30- to 350-km depth, and six sites are used across the profile.

For consistency, the CQ coefficients should be tied to the McVerry *et al.* (2000) empirical crustal anelastic attenuation coefficient, C_5 (equation 1). C_5 would be related to Q_s. We initially evaluated the $C_5(T)$ coefficients for frequency dependence of Q, considering $Q_{C5}(f) = Q_1 f^{\eta}$, and Q_1 is Q_{C5} at 1 Hz. Thus,

$$C_5(f) = -\pi f/(Q_1 f^{\eta}\ V_s). \tag{7}$$

By comparing C_5 at f = 2–13 Hz to C_5 at 1 Hz, we found that a η of 0.7 is suggested by the empirical coefficients, with η nearer to 1 for 10–13 Hz.

Synthetic t^* values are computed for varied crustal earthquakes. The frequency-independent Q_p can be matched to the crustal $Q_{C5}(f)$ by equating them at the best-fitting frequency, f_Q. The slant distance from source to site is used for r, as for other terms in the McVerry *et al.* (2000) model. However for calculating t^*, the actual 3D ray path is used. At 1 Hz,

$$t^* = r/(Q_p V_p) = r/(Q_1 f_Q^{0.7}\ V_p), \quad \text{so } Q_1^{-1} = (t^*/r)\, f_Q^{0.7}\ V_p \tag{8}$$

and the C_5 coefficient at 1 Hz can be related to the synthetic t^*,

$$C_5(1) = -\pi\ (t^*/r)\, f_Q^{0.7}\ (V_p/V_s). \tag{9}$$

The best-fitting f_Q for the synthetic crustal t^* data is 4.5 Hz.

This is a reasonable value since it is in the range (1–20 Hz) used in computing the 3D Q model. Note that f_Q is a calibration factor to relate C_5 and CQ. It would absorb any Q_p/Q_s variation without altering the CQ coefficients. For instance, if Q_p/Q_s was 1.5, f_Q would be 2.5 Hz, which is still a reasonable value.

Similarly, the anelastic attenuation coefficients for 1 Hz can be computed from synthetic t^* along any path through the 3D Q model:

$$CQ_1 = -\pi\ (t^*/r)\ f_Q^{0.7}\ (V_p/V_s). \tag{10}$$

To get CQ_1 for slab earthquakes, we use a series of sources lying along the top of the dipping subducted slab (Fig. 7). As slab seismicity is limited to a relatively narrow zone, these are representative of other events at the same depths.

The CQ_1 values for a series of sites, S1 to S6, as shown in Figure 7, are plotted as a function of depth in Figure 8. Sites S1 and S2 represent standard sites with low-loss paths as in the McVerry *et al.* (2000) model. Sites S3, S5, and S6 represent paths through the attenuating mantle wedge, but normal crust. Site S4 represents a path through both the mantle wedge and the volcanic zone, and it has over twice the attenuation rate of the standard site. The mantle wedge site, S5, also shows a very high attenuation rate.

We need simple attenuation terms for each site. Typically, for each site, there is a constant value of CQ_1 over some depth range and then a descending branch for greater centroid depths. In one case there is an ascending branch for small depths. The descending branches can be fitted by hyperbolae, as shown in Figure 8. The hyperbolae can be interpreted physically as the curves that result for travel paths through a series of regions, each with a different local attenuation rate, $\pi/(Q_1{}^*V_s)$. The local CQ_1 values of 0.0071 km^{-1} for the standard crust and lower for the deep slab implied by the following formula are confirmed by the plot of the local attenuation rates in Figure 7.

The corresponding formula give the 1-Hz attenuation coefficients.

For the standard site,

$$\begin{aligned} CQ_{1\,\mathrm{STANDARD}}(H_C) &= 0.0071 && 0\ \mathrm{km} < H_C < 60\ \mathrm{km} \\ &= 0.0025 + 0.275/H_C && 60\ \mathrm{km} < H_C < 350\ \mathrm{km}. \end{aligned} \tag{11}$$

For the mantle wedge site,

$$\begin{aligned} CQ_{1\,\mathrm{SITE}}(H_C) &= 0.0110 && 0\ \mathrm{km} < H_C < 100\ \mathrm{km} \\ &= 0.0033 + 0.77/H_C && 100\ \mathrm{km} < H_C < 220\ \mathrm{km} \\ &= 0.0025 + 0.946/H_C && 220\ \mathrm{km} < H_C < 350\ \mathrm{km}. \end{aligned} \tag{12}$$

For the mantle wedge plus volcanic zone,

$$\begin{aligned} CQ_{1\,\mathrm{SITE}}(H_C) &= 0.0088 + 0.0001\ H_C && 0\ \mathrm{km} < H_C < 60 \\ &= 0.0148 && 60\ \mathrm{km} < H_C < 100\ \mathrm{km} \\ &= 0.0025 + 1.23/H_C && 100\ \mathrm{km} < H_C < 350\ \mathrm{km}. \end{aligned} \tag{13}$$

The attenuation rates for other periods can be computed from the 1-Hz values, using a frequency exponent, η, of 0.7 and a η of 1 above 5 Hz:

$$\begin{aligned} CQ_{\mathrm{SITE}}(T,H_c) &= CQ_{1\,\mathrm{SITE}}(H_c)/T^{0.3} && T \geq 0.2\ \mathrm{sec} \\ CQ_{\mathrm{SITE}}(T,H_c) &= CQ_{1\,\mathrm{SITE}}(T = 0.2\ \mathrm{sec}, H_c) && T < 0.2\ \mathrm{sec}. \end{aligned} \tag{14}$$

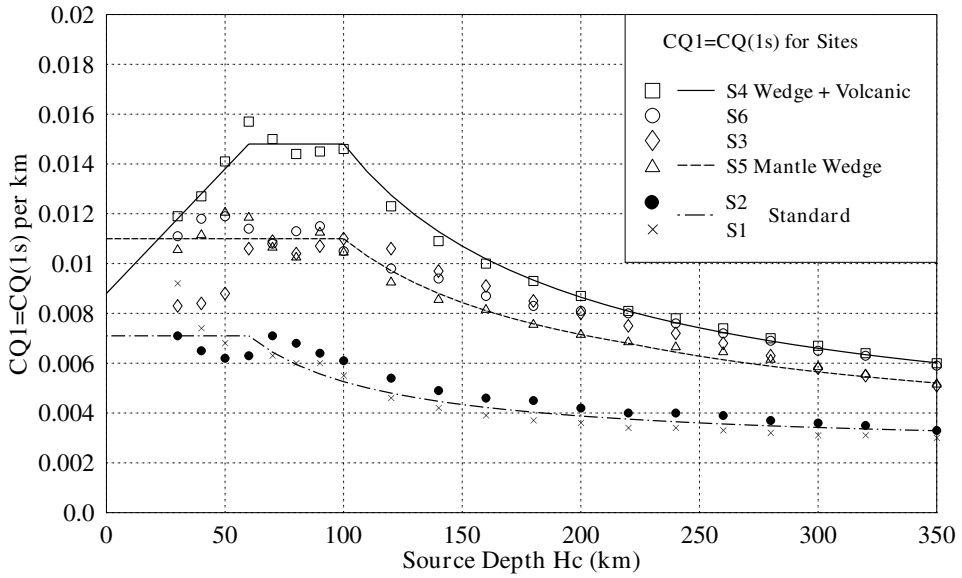

Figure 8. The average attenuation rates at 1 Hz, CQ_1, for sites S1–S6 (Fig. 7) as a function of the centroid depth (H_C) of the earthquake.

Modification to Standard Response Spectral Model

The attenuation rate term, CQ^*r, needs to be applied in a practical manner to the standard New Zealand response spectral model for subduction-zone earthquakes. The standard McVerry *et al.* (2000) subduction-zone model is based on Youngs *et al.* (1997) and provides a good fit to the available strong-motion records for slab paths to eastern stations (e.g., to stations S1 and S2; Fig. 7). As the estimates of the coefficients of the geometric attenuation term and the anelastic attenuation term tend to be strongly correlated in regression-based strong-motion models, it is not appropriate to simply add another anelastic attenuation term without redoing the regressions for the other coefficients.

Therefore the difference in the attenuation compared to the nonslab paths is added as a modification to the standard model. The slab paths to stations S1 and S2 are equivalent to the standard model paths. The difference between the attenuation rate on the standard path (i.e., to sites S1 and S2) and that on paths to sites such as S3–S6 then becomes the modification term. The form of the modified New Zealand model for subduction zone earthquakes at weak rock sites is

$$\ln \mathrm{SA}(T) = \ln \mathrm{SA}(T)_{\text{standard NZ subduction zone}} - [CQ_{\mathrm{SITE}}(T,H_C) - CQ_{\mathrm{STANDARD}}(T,H_C)]r, \quad (15)$$

where H_C is the centroid depth.

An example comparing estimated spectra for a magnitude 7.7 earthquake at 150 km depth is shown in Figure 9. The standard spectra are indicated by black lines and the modified spectra by gray lines. Sites S4 and S5 have the same standard spectra because they are the same distance. The standard and modified spectra are identical for the standard site (S2), because the path (Fig. 5) does not include low-Q zones. In contrast, both the mantle wedge (S5) and wedge-plus-volcanic (S4) sites show large decreases in acceleration spectra for the modified model, with the effect more pronounced when volcanic crust is sampled. At 0.2 sec (5 Hz), the ln SA is decreased by 1.0 for S5 and by 1.55 for S4, or SA by factors of 2.7 and 4.7, respectively.

The McVerry *et al.* (2000) model also included a volcanic-path term in the subduction-zone model for shallow subduction sources ($H_C < 50$ km), which accounts for the portion of the horizontal path that traverses the TVZ. This is compared to the CQ modified model for a 50-km-deep event in Figure 10. The two spectra for the volcanic site (S4) are nearly equivalent, because the path from 50-km depth (Fig. 7) is not sampling much of the mantle wedge and the McVerry *et al.* (2000) volcanic term produces a similar adjustment to the CQ term. For the S5 site the standard and modified spectra are quite different, with the volcanic-path

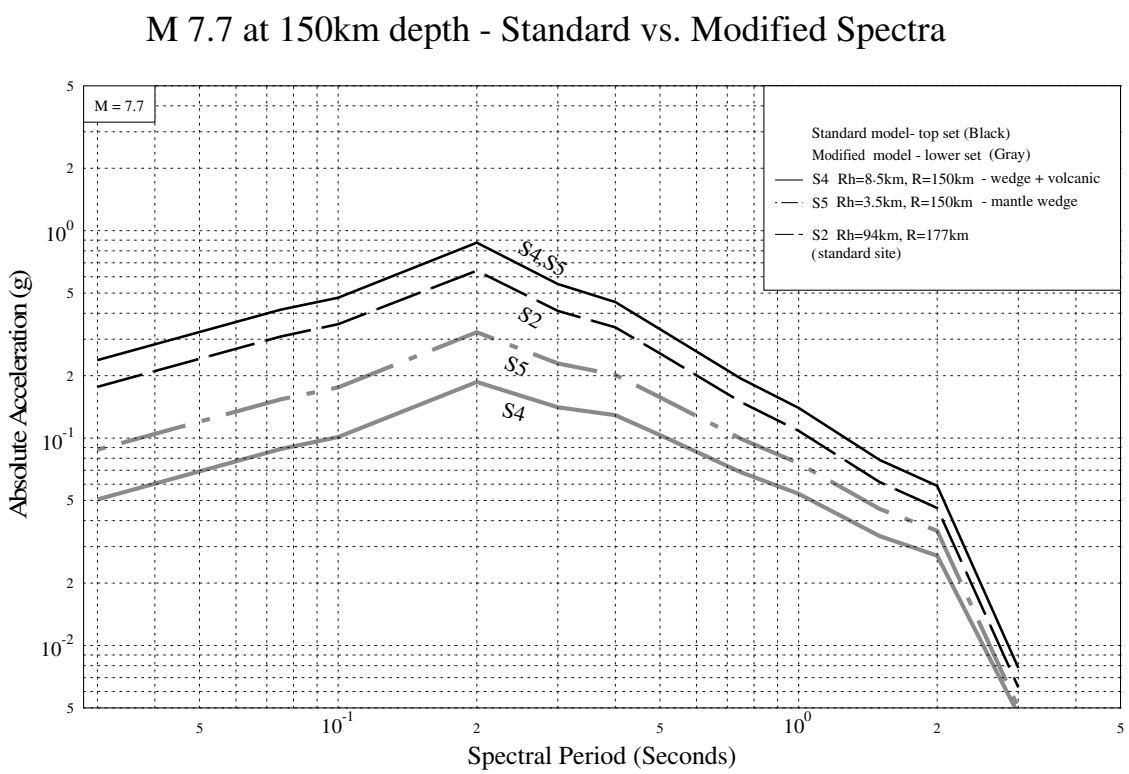

Figure 9. Comparison of spectra for a magnitude 7.7 subduction slab earthquake at a centroid depth of 150 km using the standard McVerry *et al.* (2000) model and the modified model. R is the slant distance, source to site. Note that S4 and S5 have the same R and same standard spectra and that S2 does not get modified since it is a standard site.

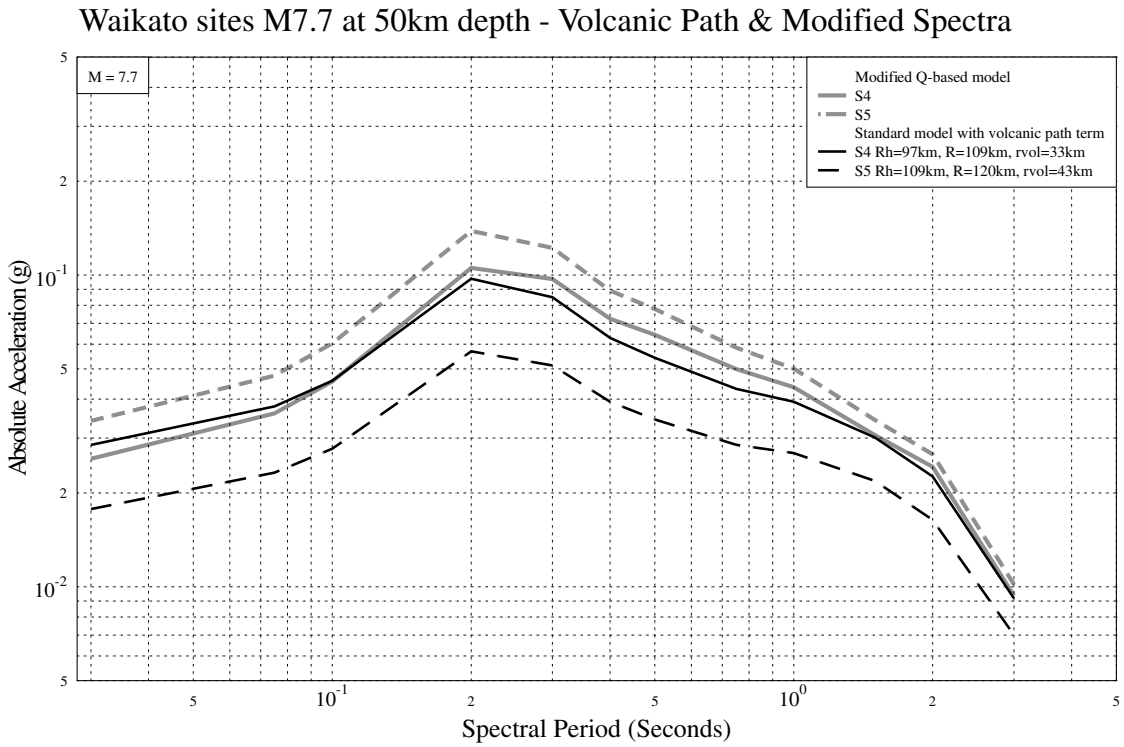

Figure 10. Comparison of modified spectra and standard McVerry *et al.* (2000) model with volcanic term included, for a 50-km-depth earthquake at sites in the volcanic zone (S4) and slightly west of the volcanic zone (S5).

term producing a larger adjustment than the *CQ* term. This is because the 3D *Q* model has a more localized shallow region of very low *Q* associated with the volcanic region, and the path from 50-km depth to site S5 largely travels below the zone of highest attenuation (Fig. 7). The exact shape of the high volcanic attenuation region is not well defined by the coarse 3D model; however it is clear that the highest attenuation is shallower than 20 km and thus the *CQ* modified model may be more appropriate for subduction-zone events than applying the volcanic path term. Hence, both for simplicity of implementation and to avoid possible overreduction of the spectra for sites with greater path lengths through the volcanic zone, it is recommended that the *CQ* modified spectra be applied for all subduction-zone earthquakes, irrespective of whether they are interface, shallow slab, or deep slab events. Thus the volcanic-path term is not included in the model (equation 15).

Acceleration Spectra for Deep Taupo Eevent

Unfortunately, the New Zealand strong-motion data set contains few records from sites affected by high attenuation in the mantle, which makes it difficult for us to demonstrate the problem addressed by our modification to the spectral attenuation model. This is partly because until the recent advent of high-resolution digital accelerographs at a few sites in the affected region, the strength of shaking in this region from deep earthquakes was generally insufficient to produce useful records. Often, the accelerographs did not even trigger in deep earthquakes that were recorded at greater distances elsewhere in the country.

One event that has produced useful records demonstrating the effect of high attenuation in the mantle was the M_w 6.0 earthquake of 25 October 1999 20:31 UTC, 161-km deep at an epicentral distance of only 18 km from Taupo. This earthquake produced records at several sites in the Napier region at epicentral distances of about 130–150 km with stronger motions (0.014*g*–0.042*g* PGA, typically around 0.017*g* PGA) than at TVZ sites closer to the source (e.g., 0.007*g* at Taupo and Reporoa, and 0.003*g* at Rotorua). Several of the Napier region records are from sites where strong amplification may have occurred from site effects. The record from the site at Napier Girls High School, on weak rock with a PGA of 0.019*g*, typical of rock and shallow stiff soil sites in the area, is selected as a representative motion of locations in the Napier area where site effects are not expected to be pronounced. Of the three TVZ records, only the Taupo record is suitable for detailed comparison.

The three-component acceleration records from Taupo and Napier are shown in Figure 11, with different scales for the accelerations. The Napier record is much stronger, with the peak value about 3 times larger, even though recorded at a distance of 213 km compared to 162 km for Taupo. The 5% damped acceleration response spectra are shown in Fig-

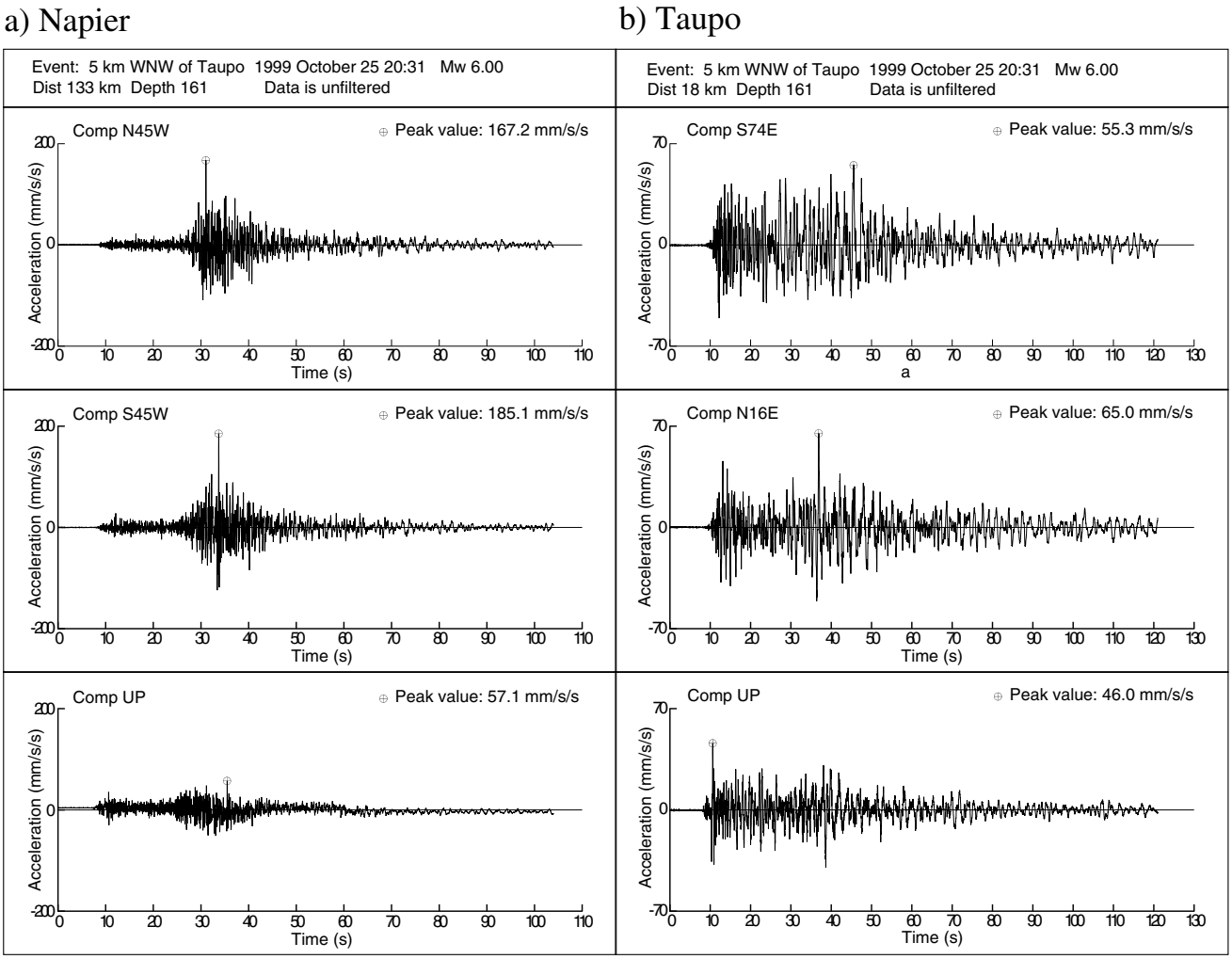

Figure 11. The three-component acceleration records from 161-km-deep earthquake, 25 October 1999, at (a) Napier and (b) Taupo stations. The peak value of each trace is noted and marked with a circled plus sign. Despite the greater distance from the source, the Napier horizontal components are about 3 times stronger than those at Taupo. Note the acceleration scale is increased for Taupo.

ure 12. As well as its higher overall amplitude, the Napier record clearly contains a relatively greater proportion of short-period (high-frequency) content, at periods less than about 0.5 sec.

The attenuated spectrum at Taupo fits the modified model very well for $f > 2.5$ Hz ($T < 0.4$ sec), which is the range used for t^* and deriving 3D Q. The observed reduction in ln SA ranges from 0.92 to 1.34. The anticipated reduction in ln SA from the modification term ranges from 0.99 to 1.22 over the 2.5 to 20-Hz range.

In comparing the waveform plots (Fig. 11), an unusual aspect is the relatively high amplitude of P relative to S at Taupo compared to Napier. The maximum of the vertical component at Taupo is a distinct arrival that comes in shortly after the direct P. Thus this is likely to be a near-source converted phase. An S to P conversion at the top of the subducted slab is a possible cause. Note that the attenuation rate once the S was converted to P would be reduced by a factor of V_p/V_s (equation 10), which would serve to exaggerate the amplitude of the converted phase.

Conclusions

The rheology of the Earth is heterogeneous in seismically active regions. This particularly influences attenuation models for deep slab earthquakes, which can, therefore, have long paths through quite different materials for different sites. Using seismograph network data, 3D Q models can be derived that image the heterogeneous attenuation.

The standard response spectral attenuation model for deep earthquakes in New Zealand overestimates spectra when the path from source to site passes through highly attenuating zones associated with the mantle wedge and TVZ. Using actual Q-values along specified paths, appropri-

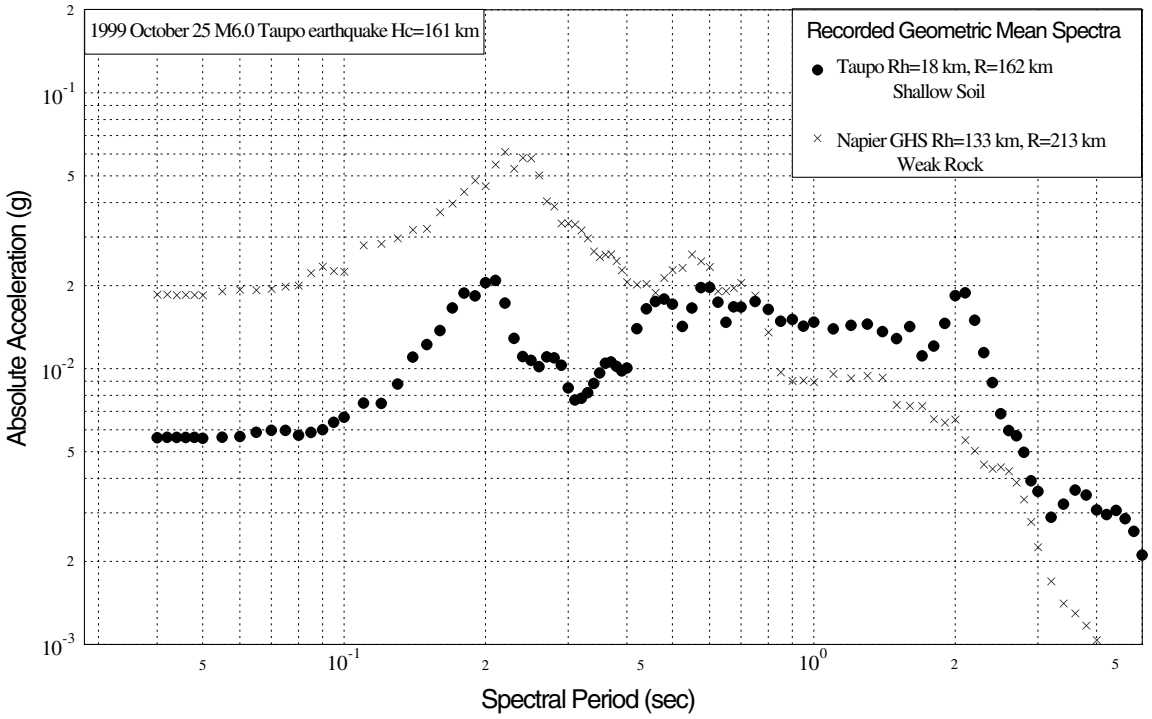

Figure 12. Comparison of Napier (crosses) and Taupo (dot) spectra for the deep earthquake shown in Figure 11. The geometric mean of the 5% damped acceleration response spectra of the two horizontal components is displayed. Note the much reduced short-period components at Taupo, with a high-loss mantle path compared to the low-loss slab path to Napier.

ate terms can be computed that modify the response spectral model to adequately model the high-loss paths for deep earthquakes. This extends the applicability of the prior model to a region lacking in strong-motion data, without having to recompute the other terms in the model. The approach may be useful in other situations where there is limited availability of strong-motion data.

The Q frequency-dependence exponent inherent in the prior model crustal attenuation term was estimated from its regression coefficients. We cannot define frequency dependence from the t^* estimates and, in reality, the frequency-dependence exponent is likely to vary with differing materials and differing attenuation mechanisms. The ductile attenuation in the mantle may be more frequency-independent Q than the attenuation in the crust. Future work would benefit from more detailed knowledge of the spatial variation of Q frequency dependence.

Acknowledgments

This work builds on the efforts of GNS seismic network staff who process the NZNSN data and maintain the database. Mark Chadwick helped with t^* analysis and plotting. We are grateful to Terry Webb, Jim Cousins, Utpal Dutta, and an anonymous reviewer for useful comments. This study was supported by the New Zealand Foundation for Research, Science, and Technology. Plots were created using GMT software (Wessel and Smith, 1998). This is Institute of Geological and Nuclear Sciences contribution 2712.

References

Abrahamson, N. A., and W. J. Silva (1997). Empirical response spectral relations for shallow crustal earthquakes, *Seism. Res. Lett.* **68,** 94–127.

Beresnev, I. A., and K. L. Wen (1996). Nonlinear soil response: a reality?, *Bull. Seism. Soc. Am.* **86,** 1964–1978.

Cousins, W. J., J. X. Zhao, and N. D. Perrin (1999). A model for the attenuation of peak ground acceleration in New Zealand based on seismograph and accelerograph data, *Bull. New Zealand Soc. Earthquake Engineering* **32,** 193–220.

Downes, G. L. (1995). Atlas of isoseismal maps of New Zealand earthquakes, Inst. Geol. Nucl. Sci. Inst. Geol. Nucl. Sci. Monograph 11.

Dowrick, D. J., and D. A. Rhoades (1999). Attenuation of modified Mercalli intensity in New Zealand earthquakes, *Bull. New Zealand Soc. Earthquake Engineering* **32,** 55–89.

Eberhart-Phillips, D., and M. Chadwick (2002). Three-dimensional attenuation model of the shallow Hikurangi subduction zone in the Raukumara Peninsula, New Zealand, *J. Geophys. Res.* **107,** ESE3, 1–15.

Eberhart-Phillips, D., M. Reyners, M. Chadwick, and J.-M. Chiu (2002). Imaging subduction zone coupling: 3-D V_p, V_p/V_s and Q in the southern North Island, New Zealand (abstract). Presented at Western Pacific Geophysical Meeting, 9–12 July, Wellington, New Zealand.

Gomberg, J. (1996). Stress/strain changes and triggered seismicity following the M_w 7.3 Landers, California, earthquake, *J. Geophys. Res.* **101,** 751–764.

Haines, A. J. (1981). A local magnitude scale for New Zealand earthquakes, *Bull. Seism. Soc. Am.* **71,** 275–294.

McVerry, G. H., J. X. Zhao, N. A. Abrahamson, and P. G. Somerville (2000). Crustal and subduction zone attenuation relations for New Zealand earthquakes. Presented at 12th World Conf. on Earthquake Engineering, 30 January–4 February, Auckland, paper 1834.

Mooney, H. M. (1970). Upper mantle inhomogeneity beneath New Zealand: seismic evidence, *J. Geophys. Res.* **75,** 285–309.

New Zealand Geomechanics Society (1988). *Guidelines for the Field Description of Soils and Rocks in Engineering Use*, New Zealand Geotechnical Society, Auckland.

Reyners, M. (1998). Plate coupling and the hazard of large subduction thrust earthquakes at the Hikurangi subduction zone, New Zealand, *New Zealand J. Geol. Geophys.* **41,** 343–354.

Rietbrock, A. (2001). *P*-wave attenuation structure in the fault area of the 1995 Kobe earthquake, *J. Geophys. Res.* **106,** 4141–4154.

Rodriguez-Marek, A., J. D. Bray, and N. Abrahamson (2001). An empirically based geotechnical seismic site response procedure, *Earthquake Spectra* **17,** 65–87.

Scherbaum, F. (1990). Combined inversion for the three-dimensional *Q* structure and source parameters using microearthquake spectra, *J. Geophys. Res.* **95,** 12,423–12,438.

Sharma, M. M., and A. N. Tutuncu (1994). Grain contact adhesion hysteresis: a mechanism for attenuation of seismic waves, *Geophys. Res. Lett.* **21,** 2323–2326.

Takai, N., H. Umeda, and S. Okada (2000). The method of predicting intensity distribution for subduction zones. Presented at Proc. 6th Int. Conf. Seismic Zonation, 12–15 November, Palm Springs, California.

Upton, P., P. Koons, and D. Eberhart-Phillips (2003). Extension and strain-partitioning in an oblique subduction zone, New Zealand: constraints from three-dimensional numerical modeling, *Tectonics* (in press).

Wessel, P., and W. H. F. Smith (1998). New version of the generic mapping tools released, *EOS* **79,** 579.

Winkler, K. W., and W. F. Murphy, III (1995). Acoustic velocity and attenuation in porous rocks, in *Rock Physics and Phase Relations: A Handbook of Physical Constants*, T. J. Ahrens (Editor), American Geophysical Union, Washington, D.C., 20–34.

Yoshimoto, K., H. Sato, and M. Ohtake (1993). Frequency-dependent attenuation of *P* and *S* waves in the Kanto area, Japan, based on the coda-normalization method, *Geophys. J. Int.* **114,** 165–174.

Youngs, R. R., S.-J. Chiou, W. J. Silva, and J. R. Humphrey (1997). Strong ground motion attenuation relationships for subduction zone earthquakes, *Seism. Res. Lett.* **68,** 58–73.

Institute of Geological and Nuclear Sciences
Private Bag 1930
Dunedin, New Zealand
(D.E.-P.)

Institute of Geological and Nuclear Sciences
P. O. Box 30368
Lower Hutt, New Zealand
(G.M.)

Manuscript received 24 February 2003.